Atmos. Chem. Phys. Discuss., 6, 7959–8009, 2006
www.atmos-chem-phys-discuss.net/6/7959/2006/

Atmospheric Chemistry and Physics Discussions

Characterizing ozone production in the Mexico City Metropolitan Area: a case study using a chemical transport model

W. Lei[1], B. de Foy[2], M. Zavala[1], R. Volkamer[1,*], and L. T. Molina[1,2]

[1]Department of Earth, Atmospheric and Planetary Sciences, Massachusetts Institute of Technology, MA, USA
[2]Molina Center for Energy and the Environment, CA, USA
[*]now at: Department of Chemistry and Biochemistry, University of California, San Diego, CA, USA

Received: 6 July 2006 – Accepted: 27 July 2006 – Published: 17 August 2006

Correspondence to: W. Lei (wflei@mit.edu)

Abstract

An episodic simulation is conducted to characterize ozone (O_3) photochemical production and investigate its sensitivity to emission changes of ozone precursors in the Mexico City Metropolitan Area (MCMA) using the Comprehensive Air Quality Model with extensions (CAMx). High O_x (O_3+NO_2) photochemical production rates of 10–80 ppb/h are predicted due to the high reactivity of volatile organic compounds (VOCs) in which alkanes, alkenes, and aromatics exert comparable contributions. The predicted ozone production efficiency is between 4–10 O_3 molecules per NO_x molecule oxidized, and increases with VOC-to-NO_2 reactivity ratio. Process apportionment analyses indicate significant outflow of pollutants such as O_3 and peroxyacetyl nitrate (PAN) from the urban area to the surrounding regional environment. PAN is not in chemical-thermal equilibrium during the photochemically active periods. Sensitivity studies of O_3 production suggest that O_3 formation in the MCMA urban region with less chemical aging (NO_z/NO_y<0.3) is VOC-limited. Both the simulated behavior of O_3 production and its sensitivities to precursors suggest that midday O_3 formation during this episode is VOC sensitive in the urban region on the basis of the current emissions inventory. More episodic studies are needed to construct a comprehensive and representative picture of the O_3 production characteristics and its response to emission controls.

1 Introduction

In recent decades, air pollution has become one of the most important and challenging problems for megacities in the world (Molina and Molina, 2004; Molina et al., 2004). Air pollution, such as high tropospheric ozone and particulates, has detrimental impacts on human health and ecosystems, and can contribute significantly to climate change. In the lower troposphere, ozone (O_3) is produced from photochemical reactions involving volatile organic compounds (VOCs, broadly including CO) and nitrogen oxides (NO_x=NO+NO_2) in the presence of sunlight. O_3 concentrations can exceed health

standards in polluted urban environments under favorable meteorological conditions (such as stagnation) and high anthropogenic emissions of NO_x and VOCs. In some urban settings biogenic hydrocarbons can also play an important role in O_3 production over regions where they contribute significantly to the total burden of emitted VOCs (Chameides et al. 1988; Kleinman et al., 2005). Tropospheric O_3 is also affected by the processes of transport, dispersion, and deposition. A prerequisite to an effective emission-based O_3 control strategy is to understand the time-and space- dependent relationship between O_3 and its precursors, and the response of O_3 concentrations to changes in emissions of NO_x and VOCs. Furthermore, an effective O_3 control strategy should include efforts to reduce O_3 production rates in areas that affect peak O_3 concentrations (Tonnesen and Denis, 2000). The ozone-precursor relationship can be understood in terms of NO_x or VOC sensitive chemistry of O_3 formation, which is usually defined based on the relative impact of a given percent reduction in NO_x relative to VOCs in the context of urban chemistry (Sillman, 1999). In this definition used in this paper, the VOC-sensitive (or VOC-limited) regime refers to conditions where a percent reduction in VOCs would lead to a significantly greater decrease in O_3 with respect to the same percent reduction in NO_x, and vice versa.

The Mexico City Metropolitan Area (MCMA) has emerged as one of the most polluted areas in the world over the last two decades (Molina and Molina, 2002). A fleet of 3.5 million vehicles in the area, together with industrial, commercial and service sources, as well as residential activities, generate high emissions of NOx, VOCs, and primary particulates to the atmosphere. In addition, the MCMA is located inside an elevated basin at an altitude of 2240 m a.s.l. surrounded by mountain ridges on the west, south and east, with a broad opening to the north and a narrow gap to the south-southwest. Because of the high altitude which makes combustion sources less efficient as well as the tropical latitude (19°25′ N), sunlight is more intense compared to low elevation, higher latitude cities. Together, these effects are more conducive for high rates of photochemical smog formation. The complex meteorological conditions associated with the complex topography in the Mexico basin also contribute to the high levels of

air pollution (Fast and Zhong, 1998; de Foy et al., 2006a). Although the air quality has improved significantly over the last decade, persistent high levels of surface O_3 and particulates are observed in the MCMA, and the national standards are often violated throughout the year (Molina and Molina, 2002; GDF, 2004).

Various field measurements have been carried out to understand the nature and causes of the air pollution problem in the MCMA (LANL/IMP, 1994; IMP 1998; Doran et al., 1998; Edgerton et al., 1999; Baumgardner et al., 2000; Raga et al., 2001). The MCMA-2003 campaign was an integrated field measurement campaign in which a wide spectrum of gas species, particles, and meteorological fields were measured (Zavala et al., 2006; Volkamer et al., 2005; Shirley et al., 2006; Salcedo et al., 2005a,b; de Foy et al., 2006a; detailed information on the campaign is also available at http://www.mce2.org). One of the goals was to improve the current understanding of the chemistry and transport processes and the evolution of pollutants in the MCMA atmosphere, and to provide insights for devising emission reduction strategies. The role of meteorology in air pollution in the MCMA has been relatively well characterized and analyzed recently through model efforts (Doran et al., 1998; Fast and Zhong, 1998; Whiteman et al., 2000; Doran and Zhong, 2000; Jazcievich et al., 2003; de Foy et al., 2005, 2006a, b). Oxidation characteristics of VOCs have also been investigated recently through measurements of secondary species and/or radical species (Gaffney et al., 1999; Marley et al., 2004; Volkamer et al., 2005; Shirley et al., 2006). Modeling studies using 3-dimensional chemical transport models (CTM) have been used to reproduce observed O_3 in MCMA (Streit and Guzman, 1996), and to identify emissions uncertainties (West et al., 2004), but few have focused on O_3 formation rates, and few comprehensive model studies have been conducted to investigate the combined roles of meteorology, chemistry, emissions and deposition in O_3 formation, spatial distribution, and temporal evolution in the MCMA (Molina and Molina, 2002; Jazcilevich et al., 2005).

In this paper, we employ a 3-D CTM, the Comprehensive Air Quality Model with extensions (CAMx), to investigate O_3 photochemical production in the MCMA and its

response to O_3 precursors. The objectives are to characterize the O_3 production rate, partition the contributions to the O_3 production of processes of chemistry, physical transformation and transport, and to evaluate the sensitivity of O_3 formation to emission reduction of anthropogenic VOCs and NO_x. A brief description of the modeling methodology is given in Sect. 2. Section 3 presents and discusses the modeling performance, in situ O_3 photochemical production, contributions of different processes to O_3 formation, and sensitivity analysis of the O_3 response to emissions reduction. A summary of conclusions and remarks are provided in Sect. 4.

2 Modeling methodology

2.1 Model and model inputs

A 3-D chemical transport model (CTM), CAMx (version 4.03), is employed for the study. CAMx is a Eulerian photochemical grid model designed to tackle air quality issues on urban and regional scales (ENVIRON, 2003). It simulates the emission, transport, chemistry, and deposition processes of pollutants in the troposphere. The model uses hourly meteorological output fields from the Penn State /National Center for Atmospheric Research (PSU/NCAR) Mesoscale Modeling System (MM5) (Grell et al., 1995), which feeds CAMx with fields of wind, temperature, water vapor, cloud/rain, land use and vertical diffusivity. The meteorological fields were simulated with MM5 (de Foy et al., 2005a), using three one-way nested grids with resolutions of 36, 12 and 3 km and 23 sigma levels in the vertical. Three-day forecasts were initialized everyday at 00:00 UTC using the Global Forecast System at a 6-h resolution. The second forecast day was used in the present work, allowing a 30-h initialization period. MM5 was run with the NOAH soil model, MRF boundary layer scheme, K-F convection scheme, simple ice microphysics, and cloud radiation scheme. The CAMx model domain (Fig. 1) is the same as the MM5 Domain 3 (D3), except that four grids were trimmed from each edge (resulting in 52×52 grid cells), with 15 vertical layers corresponding to the lowest

15 layers in the MM5, extending from the surface to 5 km a.g.l. The bottom layer interface is about 64 m a.g.l. The chemical initial and boundary conditions were similar to those used in West et al. (2004), except that lower VOC and CO values were used for the boundary conditions, and the north boundary was treated the same as the other boundaries because of a broader domain than the CIT domain used by West et al. (see Fig. 1). The SAPRC99 gas phase chemical mechanism (Carter, 2000) was used. Photolysis rate frequencies for clear sky were precomputed with the Tropospheric Ultraviolet and Visible radiation model (TUV, Madronich and Flocke, 1998). In the computation, the aerosol loading was scaled to match those measured in the MCMA-2003. In the highly polluted area the aerosol optical depth at 340 nm wavelength was set to 0.8, comparable with the concurrent LIDAR aerosol extinction measurements (S. Frey, private communication, 2004). The effects of cloud presence on photolysis rates were accounted for by using the approach of Chang et al. (1987).

2.2 Emission estimates

The emission input was constructed based on the official emissions inventory (EI) for the MCMA in 2002 (CAM, 2004). Total annual emitted masses of VOCs, CO and NO_x were distributed across mobile, point and area source categories considered in the emission inventory and were transformed into spatially and temporally resolved and chemically speciated emission fields following the databases and procedures in West et al. (2004). The databases and procedures were updated ever since wherever possible. In particular, upgrades of the spatial distribution of mobile and area source emission fields were performed using a grid resolution of 2.25 km, in which more detailed road type information in each grid cell and improved population distribution were taken into account. The emission input constructed above is referred to as the initial emission estimates thereafter. A summary of the total basin wide emissions by source category and pollutant type is given in Table 1 and a map of MCMA CO, NO_x and VOC emissions are shown in Fig. 2.

It has been suggested that the VOC emissions in the current EI in the MCMA were

underestimated by as much as a factor of 2–3 (Molina and Molina, 2002; Arriaga-Colina et al., 2004; West et al., 2004). Underestimates of VOC emissions by a factor of 2 or more has also been a typical phenomenon in the U.S. (Sillman, 1999; Russell and Dennis, 2000). An extensive array of VOC measurements were obtained during the MCMA-2003 campaign using a variety of techniques, including canister sampling analyzed by Gas Chromatography/Flame Ionization Detection (GC-FID), long path differential optical absorption spectroscopy (DOAS) measurements, FTIR and PTRMS measurements (Velasco et al., 2006; Volkamer et al., 2005; Rogers et al., 2006). On the basis of the initial emission estimates, model runs were carried out, and modeled VOC (as well as NO_x and CO) concentrations were compared with the extensive suite of VOC measurements of the GC-FID and DOAS (the PTRMS data were not used due to the commensurability difficulty in species lumping). The initial emission estimates were adjusted such that a satisfactory agreement in the comparisons was reached (see details in Sect. 3.1 for the comparisons). Scaling factors (mole based) as listed in Table 2 were applied to the initial emission estimates. These adjustment factors were similar to those reported by Velasco et al. (2006), who used the distribution of measured ambient concentrations from canister sampling to estimate adjustments in the distribution of emissions by species classes. The factors in Table 2 are different from those given by Velasco et al. because different speciation methods were used and because different base year inventories (1998 vs. 2002) were employed (for example, ALK2 in Velasco et al. corresponds to ALK5 in this paper, and ALK1 in the former is mainly a combination of ALK2, ALK3 and ALK4 in this paper). Also included in Table 2 are the adjustment factors for aldehydes in which primary sources make significant contributions (Garcia et al., 2005) in MCMA. Kolb et al. (2004) and Zavala et al. (2006) suggested that vehicle emissions of formaldehyde (HCHO) in the MCMA may be higher than previously reported, which was estimated based on the emission rates and speciation profiles in U.S. urban cities. Primary formaldehyde may significantly influence radical budgets and photochemistry in the MCMA. Based on the comparison of model-DOAS measurements at CENICA (see Sect. 3.1), emissions of HCHO were

scaled by a factor of 9, and a scaling factor of 4 was assumed for higher aldehydes. Both the emission rates (in the initial emission estimates) and photolysis rates of the higher aldehydes are much lower than those of HCHO, and thus their role in the photochemistry is not as significant as HCHO in the MCMA. The adjusted VOC emissions are also summarized in Table 1. The total VOC emissions increase about 65% (mass based) after the adjustment, which is still lower than the previous estimates of a factor of 2 to 3.

Weekend and day-to-day emission variations were also considered. It was assumed that, based on traffic count information and an analysis of the variation of morning peak CO concentrations, vehicular emissions decreased by about 10% on Saturday and 30% on Sunday (Garcia, A. and de Foy, B., private communication, 2005). The modeling episode (see the section below) includes part of Easter week, in which schools were closed and residents left the city for vacation. As shown in ambient concentrations and measured fluxes (Velasco et al., 2005, 2006), emissions were reduced during the holiday week. Based on the RAMA CO measurements, emissions during these days were downscaled by 10% of regular days. This adjusted emission scenario is defined as the reference case in this paper.

2.3 Episode selection

A 4-day episode of 13–16 April 2003 was chosen for this study. The model was started at 12 April 00:00 Z allowing 24 h for spin-up to reduce the influence of initial conditions. We chose this period because it was an "O_3-South" episode in the MCMA (de Foy et al., 2006a). In "O_3-South" days, meteorological conditions are characterized by weak synoptic forcing, stagnant surface winds and clear skies, which is conductive to the occurrence of high O_3 levels. In addition, The "O_3-South" episode is a typical meteorological phenomenon in the MCMA, and these meteorological conditions have been extensively studied (Williams et al., 1995; Fast and Zhong, 1998; Whiteman et al., 2000; de Foy et al., 2006a). On "O_3 -South" days, the MCMA basin flow is governed by a thermally-driven northerly flow from the Mexican plateau during the day, southerly

gap flow from the southeast passage in the late afternoon and early evening, which leads to the highest O_3 levels in the south of the city (de Foy et al., 2006a).

As note above, the Easter Week started on 14 April and traffic counts and pollutant concentration were about 10% less than during other weeks (Garcia et al., 2005). Although the emissions scenario for this episode were slightly less than during a non-holiday period, we believe the episode can be used to represent normal day scenario for MCMA, given the O_3 patterns that occurred.

3 Results and discussions

The model performance during this study episode is evaluated initially by comparing near surface O_3, NO_x and CO with measurements from the Ambient Air Monitoring Network of Mexico City (RAMA) and by comparing VOC concentrations with measurements/analyses from canister data (Velasco et al., 2006) and DOAS (Volkamer et al., 2005) at CENICA. The characteristics of O_3 photochemical formation are discussed next. Finally, the O_3 response to precursor emission reductions is presented.

3.1 Model performance

The MM5 performance has been described by de Foy et al. (2005, 2006b). The main features of the Mexico basin flow are well represented by the model including the northerly flow from the Mexican plateau during the day, up-slope flows on the basin edges and the southerly gap flow from the southeast passage in the late afternoon and early evening. Weak synoptic forcing leads to surface winds that are weak and variable and particularly challenging to model. The main difference between the model and the observations is the timing of the increase in surface wind speeds and the wind shift. This affects the location of the horizontal wind convergence zone which can have a large impact on pollutant dispersion predictions.

The model performance of CAMx is evaluated by comparisons of near-surface con-

centrations of O_3, CO, NO_x, and VOCs with a comprehensive suite of measurements. First, modeled hourly concentrations of O_3 in the bottom model layer (0–64 m) are compared with the RAMA measurements. Figure 3 shows the comparison of surface peak O_3 concentration and its geographic distribution. The period of 13–16 April was an "O_3-South" episode. Specifically, a transition from "O_3-North" to "O_3-South" occurred on 13 April, with the peak O_3 located in a narrow strip running SW–NE through the city center. Subsequently, peak O_3 concentrations occurred in the south of the city. In general, the model reproduces the spatial distribution and magnitude of peak O_3 reasonably well (considering the affecting factors discussed below), although in some stations the peak O_3 concentrations are off by a factor of 2. The main discrepancy is that the modeled O_3 center is shifted far to the south of the city and the O_3 peak levels are overestimated. In particular, on 16 April the predicted O_3 peak is too far to the south of the city. On the other hand, predicted NO_x concentrations (not shown) during morning rush hours are in excellent agreement with the RAMA measurements. The agreement between the predicted and observed distribution of NO_x concentrations suggests that the misplacement of peak O_3 is not due to the spatial representation of pollutant emissions. One cause is probably the simulated meteorological factors mentioned previously. For example, as mentioned above, weak and variable surface winds, which are difficult to simulate and yet to which O_3 concentration and its spatial distribution on the urban scale are very sensitive, may contribute to this. In addition, the discrepancy of simulated sharp wind shift from south-easterly to north-westerly in the morning vs. the observed gradual turning (see Fig. 15 in de Foy et al., 2006b) probably also contribute to the misplacement. Another factor may be associated with the treatment of HONO chemistry and other missing radical sources in the current SAPRC99 gas-phase chemical mechanism. Recently both laboratory studies and field measurements have reported that the heterogeneous chemistry is a major source of nighttime HONO (Kleffmann et al., 1998; Finlayson-Pitts et al., 2003; Stutz et al., 2004), even though their mechanisms on the molecular level still remain a mystery. Acker et al. (2006) reports daytime HONO primary sources in rural areas. In the current SAPRC99 mech-

anism, the association reaction of OH+NO+M→HONO+M is the sole source of HONO in the atmosphere, which is not able to explain the nighttime accumulation of HONO concentration up to a few ppb observed during the MCMA-2003 campaign (Volkamer et al., 2006[1]). HONO is an important morning radical source in the MCMA (Volkamer et al., 2006[1]). Our simulation tests over several episodes using the base case emissions (adjusted day-to-day based on the traffic count information) indicated (not shown) that the model using the current SAPRC99 mechanism resulted in delayed and underpredicted radical concentrations in the high NO_x MCMA area, leading us to the suspect of missing radical sources or/and missing NO_x sinks in the mechanism. The missing HONO sources and possible missing and delayed other radical sources can lead to the delay of O_3 formation and the shift of high O_3 center to the downwind regions; missing NO_x sinks can lead to overprediction of peak O_3. We are under way to numerically investigate the radical chemistry in the MCMA.

There are several stations where very local NO_x emissions reduce the peak O_3 concentrations; for example see station EAC in Fig. 1 and Fig. 3. Based upon these reduced O_3 peaks, we chose eight monitoring stations for the model-measurement comparison. These eight stations, denoted as the REP-8 stations thereafter were distributed throughout urban area (see Fig. 1). Figure 4 compares measured and simulated concentrations of O_3, NO_x, and CO averaged over the REP-8 stations. Measurements of NO_x from RAMA using the chemiluminescence technique more accurately represent NO_y (NO_x+NO_x oxidation products). Accordingly we compared the RAMA NOx measurements with the sum of model species corresponding to NO_y. NO_x involved in comparisons with the RAMA measurements thereafter in this paper is also in fact NO_y. The model reproduces correctly the diurnal variation of O_3 in the first 3 days, although the peak O_3 on 14 April is overestimated (by about 30 ppb). On 16 April, peak O_3 is underestimated by about a factor of 2 and the O_3 center was shifted too far to the south of the city. Because of this, analyses and discussions of photochemical

[1]Volkamer, R., Sheehy, P., Molina, L. T., et al.: Experimental quantification of the primary and secondary HO_x formation in Mexico City, in preparation, 2006.

characteristics of O_3 formation below will not include data from 16 April.

Comparison between observed and simulated species concentrations can also provide information on the accuracy of emissions estimates. Figure 4 shows that simulated NO_x and CO agree well with the measurements, and there are no systematic biases between modeled and observed daytime NO_x and CO, even though there appear to be some hangovers of simulated NO_x and CO during midnight and very early morning. The hangover of CO can be explained by the underprediction of nighttime vertical mixing and boundary layer (PBL) height. NO_x has larger hangovers than CO, most of which is contributed by overpredicted NO_2 during that period, not due to the accumulation of emitted NO. This gives us confidence in model performance and in the accuracy of the emissions of CO and NO_x used in the model. The overprediction of nighttime NO_2 is probably an indication of possible missing sinks of NO_x at high NO_x urban environments.

We compare predicted VOC species with a comprehensive array of available observations that were described in detail in Velasco et al. (2006) and Volkamer et al. (2005). Figure 5a compares predicted concentrations of alkenes and speciated alkanes from canister samples measured and reported in Velasco et al. (2006). The adjustment factors presented in Table 2 have been used in the model. The predicted alkene and alkane concentrations agree well with the measurements. Note that the canister data are 30-min averages while the simulations represent 1-h averages. Figure 5b shows the comparison of predicted concentrations of aromatics and formaldehyde with those measured by DOAS. Observed ARO1 was constructed from the DOAS measurements of toluene and benzene, and observed ARO2 was derived from DOAS measurements of xylenes using a scaling factor. The scaling factor used for estimating the DOAS ARO2 was obtained from the canister data in which the contribution of xylenes to ARO2 can be estimated. Again a good agreement between predictions and measurements are found for aromatics on 14–15 April, and no systematic bias exists. Measured aromatic concentrations on 13 April are much higher than the rest of the period, which the model is not able to reproduce. However the phenomenon of much higher predicted

aromatic concentrations on 13 April than on other days is not found in CO or NO_x, nor in HCHO. HCHO during the morning hours is somewhat underestimated at CENICA even with an adjustment factor of 9 to the HCHO emissions. Nevertheless grid cells a few kilometers north and west of CENICA were predicted to have much higher HCHO concentrations. Figure 5b includes the simulated HCHO concentrations at the model grid 3 km northwest of CENICA (dashed line), which gives similar peak HCHO concentrations as the DOAS observations at CENICA. This may suggest an uncertainty in the spatial distribution of the HCHO in the EI, considering the fact that CENICA is on the edge of the high vehicular emission area in the current emission inventory. For example the total emission estimates may need to be allocated over a broader area considering the growth of the city.

Based on these comparisons, it seems that emissions of some VOC species are underestimated by a factor of 2–3 in the EI, but not all VOCs are underestimated (overall the emissions of VOCs are underestimated by about 65%). This result is consistent with the conclusions of Velasco et al. (2006) that are based on the canister-EI comparisons of early morning VOC abundance. It should be noted, however, that the adjustments of VOC emissions were solely based on comparisons at only one station (CENICA), over a few days (one day for alkanes and alkenes), with limited dataset, and with assumptions that the spatial and temporal distribution of emissions in the EI were accurate. To thoroughly evaluate the uncertainty of EI, more investigations are needed including comparisons with broader spatial and temporal coverage.

3.2 Photochemical formation rate and production efficiency

3.2.1 Theoretical background

O_3 formation can be considered a radical competition process in which VOCs and NO_x compete for the OH radical (Seinfeld and Pandis, 1998). When NO_x increases, passing the turnaround level, defined as the NO_x level at which $P(O_x)$ reaches a maximum, $P(O_x)$ is expected to decrease (Sillman et al., 1990; Kleinman et al., 1997; Daum

et al., 2000). Based on the concept of radical budget ($OH+HO_2+RO_2$), Sillman et al. (1990), Kleinman et al. (1997), and Daum et al. (2000) derived analytical solutions for O_3 photochemical production in terms of O_3 precursors and other oxidation products that can be readily measured. These analytical equations have been widely used in box models to calculate O_3 production rates based on observations. These approximate equations are

$$P_G(O_3) = \frac{k_t}{\sqrt{2k_{\text{eff}}}} \sqrt{Q - L_N - L_R}[NO] \quad (1)$$

$$P_G(O_3) = Y \frac{k_{OH-VOC}[VOC]}{k_{OH-NO2}[NO_2]} (Q - 2PFR - L_R - L_N), [NO_x] > \sim 1\ \text{ppb} \quad (2)$$

where k_t is the weighted average rate constant for reaction of HO_2 and RO_2 with NO, k_{eff} is the effective rate constant for peroxide (H_2O_2+ROOH) formation, Y is the average yield of $[HO_2]+[RO_2]$ for each OH+VOC reaction, k_{OH-VOC} and k_{OH-NO2} are the rates constants of reactions of VOC+OH and NO_2+OH, respectively. Other notations are listed in Table 3. Note here Q is the production rate of primary radicals (i.e., radicals generated from the radical initiation, not those participating in the radical propagation. The primary radicals here are not necessarily associated with direct emissions), which is determined largely by the photolysis of O_3, aldehydes and other intermediate VOCs (including those from VOC oxidations and direct emitters).

Equation (1) assumes that the O_3 production rate is the rate of NO oxidation to NO_2 by peroxy radicals (i.e., NO_x limited). Thus, Eq. (1) is suitable for examining the behavior of $P(O_x)$ at low NO_x concentrations. Inherent to Eq. (2) is the assumption that the O_3 production rate can be approximated by the rate at which OH reacts with VOCs (i.e., VOC limited). Equation (2) is thus most appropriate for examining the behavior of $P(O_x)$ at NO_x-abundant conditions. An implicit assumption in deriving Eq. (2) is that no primary peroxy radicals contribute to the O_3 production (the Q term is introduced into Eq. (2) because of the need to represent [OH] using other species on the basis of radical budget).

Subtracting the O_3 chemical loss term from $P_G(O_3)$ gives the net O_3 chemical formation rate ($P(O_3)$) (analogously for $P(O_x)$). Under urban conditions the O_3 chemical loss term is usually much smaller than the gross production term. For example, simulations of several different episodes in the MCMA indicated that near surface O_3 chemical loss was constantly about 7–9% of the gross chemical formation in the afternoon. Therefore Eqs. (1–2) are also good approximations for $P(O_3)$. Under urban conditions radical losses due to radical-radical reactions (PFR and L_R) are very small compared to other loss pathways such as formations of HNO_3, PANs and other organic nitrates (c.f. Fig. 7f below). Thus Eq. (2) can be further simplified as

$$P_G(O_3) = Y \frac{k_{OH-VOC}[VOC]}{k_{OH-NO2}[NO_2]}(Q - L_N), [NO_x] >\sim 1 \text{ ppb} \quad (3)$$

These equations will be employed to discuss the $P(O_3)$ in the MCMA in the next section.

3.2.2 Characteristics of ozone production rate

It is important to determine the relationship between O_3 formation and O_3 precursors in order to understand O_3 formation and response of O_3 to emission control strategies. We examined the net photochemical formation rates of O_x (=O_3+NO_2 in this paper), $P(O_x)$, as a function of NO_x; the results are presented in Fig. 6. O_x is used instead of O_3 because O_x is a more conservative quantity than O_3 in that it is not influenced by the titration process of $NO+O_3 \rightarrow NO_2$. In Fig. 6, model data sampled within the urban region (as shown in Fig. 1) between 12:00–17:00 CDT during 13–15 April are used. The time window of 12:00–17:00 CDT is when the most active O_3 production and the O_3 peak occur. In the calculation $P(O_x)$ includes chemical losses of NO_x to gaseous HNO_3, PANs and other organic nitrates. $P(O_x)$ can be a good approximation for $P(O_3)$ (net ozone photochemical production rate) because $P(NO_2)$ is expected to be small compared to $P(O_3)$ due to the rapid inter-conversion between NO and NO_2 in this time window. Note that the $P(O_x)$ output from the CAMx model is an hourly-cumulative quantity, not the instantaneous production rate. A distinct feature in Fig. 6

is the large scatter relationship between $P(O_x)$ and NO_x. Near-surface NO_x concentrations vary between 10 and 80 ppb, and consequently values of $P(O_x)$ vary between 10 and 80 ppb/h. The model values and the scatter in the dependence of $P(O_x)$ on NO_x is consistent with observation-based estimates of $P(O_3)$ (Shirley et al., 2006). In addition, in the MCMA no obvious turnaround behavior of $P(O_x)$ can be deduced based on Fig. 6, even when NO_x concentration reach as high as 100 ppb. Despite the scatter in the relationship, the mean values of $P(O_x)$ at each NO_x level are much higher than in most U.S. urban regions (Kleinman et al., 2005), even at very high NO_x levels, and are close to or higher than those found in the Houston metropolitan area (Kleinman et al., 2002; Lei et al., 2004).

Figure 7 shows the relationship among $P(O_x)$, primary radical source (Q, in unit of ppb/h), and VOC-to-NO_2 reactivity. $P(O_x)$ is nearly a linear function of the square root of primary radical production rate (Fig. 7c), i.e., $P(O_x)$ is predominantly determined by the availability of primary radicals. Therefore the scatter in the relationship shown in Fig. 6 reflects the dependence of the radical source on NO_x. $P(O_x)$ is weakly dependent on $\sqrt{Q - L_N}[NO]$ (not shown). We can therefore conclude that Eq. (1) can not be applied to explain the $P(O_x)$ behavior in the MCMA, i.e., O_x production is not NO_x limited. Instead, Eq. (3) explains the $P(O_x)$ behavior well (Fig. 7d), i.e. P(Ox) is largely determined by the radical source and the VOC-NO_2 reactivity ratio. This implies that O_x formation is VOC limited. About 18% of the sampled data points deviate from the linear cluster (located beneath the cluster), which is probably due to the non-inclusion of the contribution of primary peroxy radical sources to the O_3 production in Eq. (3). HCHO has been quantified as an important radical source in the MCMA (Volkamer et al., 2006[1]). The primary peroxy radicals may have significantly influenced a small portion of the sampled data in Fig. 7. Including the contribution of primary peroxy radicals to O_3 production would increase $P(O_x)$, and thus improve the "clustering" in Fig. 7d. Figure 7d (the slope) also shows that on average two peroxy radicals are yielded for each OH+VOC reaction. We also note that P(Ox) is affected significantly by the L_N term, suggesting the importance of the formation of PANs and other organic

nitrates in the photochemical process. The VOC-to-NO_x reactivity ratio contributes to the magnitude of $P(O_x)$, but no apparent dependences are found between the reactivity ratio and $P(O_x)$ (Fig. 7b). The relatively constant ratios of VOC-to-NO_x reactivity (~3–6) in Fig. 7b suggest the co-location of emissions of NO_x and VOCs in the MCMA. The radical source increases with VOC reactivity (Fig. 7e), so does the O_x production (Fig. 7a). Figures 7c, d and e indicate that VOC reactivity plays an essential role in the O_x photochemical production. During this period, over 90% of radicals are lost to the NO_x oxidation while less than 10% are lost to the radical-radical reactions (Fig. 7f), implying that the O_x formation is VOC limited (Sillman et al., 1995; Kleinman et al., 1997).

In summary, during photochemical active period of 12:00–17:00 CDT $P(O_x)$ depends not only on NO_x (and sunlight of course), but also on VOC reactivity and primary radical sources; NO_x losses to PANs and other organic nitrates also affect $P(O_x)$. Therefore no simple relationship between $P(O_x)$ and NO_x is found. However, the dependence of $P(O_x)$ on precursors is controlled by the primary radical source, which in turn is dependent on the VOC reactivity. The relationship between $P(O_x)$ and precursors and the primary radical source suggests that O_3 formation in the urban region is VOC-limited during this period.

3.2.3 VOC reactivity partitioning

As discussed above, the VOC reactivity plays an essential role in determining the O_x photochemical formation. A further effort is made to examine the apportionment of VOC reactivity. Figure 8 illustrates the contributions of various VOCs to the VOC reactivity in the afternoon. The calculated total VOC reactivity is very high with mean values $>15\,s^{-1}$, which is close to the values observed in plumes over the Houston Ship Channel area (Kleinman et al., 2002; Daum et al, 2003), and much higher than other U.S. urban environments (Kleinman et al., 2002, 2005; Lei et al., 2004). Including the contribution from CO, the total reactivity (about $20\,s^{-1}$) is in very good agreement with the observed OH reactivity) by Shirley et al. (2006) (although the latter includes OH

loss to other chemical processes, e.g., OH+NO_2 for the same time window). Alkanes, alkenes and aromatics make comparable contributions to the VOC reactivity, with alkanes slightly dominating. Velasco et al. (2006) report that during the early morning rush hour, alkenes dominate the total VOC reactivity in the MCMA. As time evolves, relatively less contribution to the VOC reactivity would be expected from the more reactive alkenes in the afternoon due to their shorter lifetimes. An important feature in Fig. 8 is that aromatics make a significant contribution, in which aromatic compounds with high reactivity, such as xylenes, account for about 75% of the aromatic activity (not shown). This is unique compared to most urban cities in U.S. where either alkanes or alkenes contribute the majority of VOC reactivity. Aromatics are important precursors for secondary organic aerosols (Odum et al., 1996; Seinfeld and Pandis, 1998). The importance of aromatics to the VOC reactivity may have important implications in formulating effective control strategies for the VOC-limited area, because reduction in aromatic emissions may lead to significant decrease in both O_3 and organic aerosols, and thus reducing the emissions of aromatics may help to bring nonattainment areas into complying with the national standards for O_3 and particulates. Aldehydes, mainly the intermediate oxidation products of primary VOCs, also contribute as much as other primary VOCs, furthering the O_3 production potentials of primary VOCs. Another noticeable feature is the role of CO in the OH reactivity due to the very high concentrations of CO observed in the MCMA. The high VOC reactivity contributes to the lack of turnaround behavior of $P(O_x)$ shown in Fig. 6.

3.2.4 Characteristics of ozone production efficiency

Ozone production efficiency (OPE) is defined here as the number of O_3 molecules generated photochemically per NO_x molecule oxidized (i.e., $P(O_3)/P(NO_z)$. NO_z is the oxidation products of NO_x, NO_z=NO_y–NO_x). OPE is an important metric for understanding O_3 formation and response to precursor emissions control. It contains information about the conditions under which O_3 is produced and is important in evaluating impacts from NO_x emission sources. OPE determines the efficiency of the catalyst

NO_x in the O_3 formation. In this study, OPE is approximated as $P(O_x)/P(NO_z)$. Under conditions where the O_3 titration does not significantly affect the O_3 production, such an approximation is valid. Figure 9 presents the predicted afternoon hour near surface OPE as a function of NO_x in the MCMA. Over this time window (12:00–17:00 CDT) $P(O_x)/P(NO_z)$ is expected to be a good approximation of the OPE. In the calculation of NO_x oxidation rate, $P(NO_z)$, HNO_3 formation from the reaction of $OH+NO_2$ and net formation of organic nitrates (including PANs), the predominant terms, are included; no other minor terms such as deposition and particulate NO_3^- heterogeneous removal are considered. The calculated values of OPE frequently concentrate on 4-12 molecules of O_3 per NO_x oxidized at NO_x>10 ppb, which are higher than in those observation-based or modeled in urban plumes of most U.S. urban cities in the same NO_x range, such as New York City (3–4) (Kleinman et al., 2000); Nashville (3–6) (St. John et al., 1998; Nunnermacker et al., 1998), Phoenix (3–5) (Kleinman et al., 2002), and Houston (3–8) (Kleinman et al., 2003; Lei et al., 2004), particularly at higher NO_x levels. From Eq. (2) (divided by Q, note that $Q \approx P(NO_z)$ shown in Fig. 7f), we can find that the OPE values are closely related to the VOC-to-NO_2 reactivity ratio, and OPE increases with increases in the ratio. A nonlinear dependence of OPE on NO_x is also exhibited, as found by Liu et al. (1987).

3.3 Process apportioning of ozone production in the boundary layer

O_3 production is the result of the interaction of the emission, chemistry, transport and deposition processes. 3-D CTMs are probably the most powerful tool to gain an understanding of these interacting processes. The Process Analysis (PA) tool in CAMx is employed to apportion the O_3 production from these processes. Figure 10a presents the time series of contributions of these processes to O_3 formation in the MCMA urban region in the boundary layer. The nighttime mixing layer height was assumed to be 500 m deep, close to the upper limit of observations. In general, O_3 is produced photochemically during the day. The photochemical formation starts at 10:00–11:00 CDT, enhances significantly after 11:00 CDT and rapidly reaches maximum during 12:00–

14:00 CDT. As a maximum reaches, ozone is transported to the free troposphere via vertical advection; on 15 April it is also transported to the surrounding environment through bilateral advection. The outflow to the free troposphere is usually accompanied by inflow through the horizontal advection to preserve the mass conservation of the air mass. The outflow of urban pollution suggests a regional-scale air quality impact.

Both the enhancement time and peak time are about 1 h earlier than that for O_3 concentration itself, but is about 1–2 h later than the observation-constrained near surface $P(O_3)$ (Shirley et al., 2006). Although there are many factors contributing to this discrepancy, such as the difference in height (PBL vs. surface), and geographical coverage (urban area average vs. one site), the determining factor is probably due to the missing reactivity and radical sources at high NO_x conditions for the chemical mechanism employed in the model as discussed previously. Carter (2005) suspects that the current mechanism for aromatics (an important VOC species in the MCMA, see Fig. 8) in SAPRC99 underpredicts radical inputs, which leads to the underprediction of O_3 formation in the VOC-limited environments.

Dry deposition can be important for O_3 removal in the near surface (reaching ~7 ppb/h on the diurnal average basis), but for the entire PBL, its effects are negligible.

We also conduct a similar analysis for PAN. PAN can be an important reservoir species for NO_x and radicals in less-polluted tropospheric regions. The partitioning results are presented in Fig. 10b, which reveals two important features. First, PAN is not in chemical-thermal equilibrium during the photochemically active period. This is demonstrated by the positive net chemical/thermal production of PAN throughout the daytime period, with a production rate as high as 2 ppb/h occurring in the mixing layer. This is opposite to results from many urban environments. Gaffney et al. (1999) reported very high PAN concentrations in the MCMA, which they attributed to the high levels of PAN precursors. The non-equilibrium state of PAN may also contribute to the high PAN levels. Second, significant amounts of PAN are transported to regional am-

bient air. This again suggests that outflows of pollutants in the MCMA may affect the ambient air quality and photochemistry on a regional scale. We expect that significant amounts of pollutants and primary pollutant precursors be transported out of the city to the regional environment.

3.4 Sensitivity of O_3 formation to precursors

High levels of ozone are produced in the urban area due to anthropogenic emissions of NO_x and anthropogenic and biogenic emissions of VOCs. A key issue in developing an effective O_3 control strategy is to understand the nonlinear relationship between O_3 and its precursors. In this section we evaluate the response of O_3 levels to the O_3 precursors by perturbing the emission rates and comparing the resulting changes in O_3 concentrations and O_3 photochemical production rates with the reference run. The perturbations of emissions include a 50% reduction in NO_x emissions, a 50% reduction in VOC emissions, and a 50% reduction in both NO_x and VOCs emissions.

Figure 11 illustrates the effects of emissions reductions on near-surface O_3 averaged over the REP-8 stations. It clearly shows that a 50% reduction in NO_x emissions leads to little decrease in O_3 (on 13 April), or even increases in O_3 (on 14–15 April), while a 50% reduction in VOC emissions results in decreases of O_3 by nearly a factor of two. 50% reductions in emissions of both NO_x and VOCs also lead to a decrease in O_3, but less than the VOC-only scenario. Emission reductions also affect the timing of O_3 formation: the reduction in NO_x emissions causes the peak O_3 to form one hour earlier and the morning-hour O_3 to rise more rapidly and efficiently; the reduction in VOC emissions leads to a one-hour delay in the timing of peak O_3 and delays the rise in the morning-hour O_3. The accelerated and enhanced O_3 formation in the NO_x-reduction case (with respect to the base case) on 14–15 April is indicative of the O_3 VOC-sensitive chemistry in the midday during this period. The NO_x-reduction case also indicates O_3 sensitivity evolves along the day. For example, on 14 April, with the reduction of NOx emissions, O_3 increases in the morning while it decreases in the late afternoon and increases again in the evening. This concurs with the findings of Molina

et al. (2002), in which detailed analyses of the evolution of O_3 sensitivity to precursors were presented.

The geographic distribution of the change of $P(O_x)$, averaged over 12:00–17:00 p.m., due to a 50% reduction in NO_x emissions on 15 April 2003 are shown in Fig. 12. $P(O_x)$ is used over O_x is because $P(O_x)$ represents instantaneous ozone chemistry that would apply to a broad range of atmospheric conditions and is less dependent on assumptions on individual calculations (Sillman, 1999). The reduction of NO_x emissions leads to increases of $P(O_x)$ in most of the urban area, particularly in the southern urban area, where peak O_3 increases more than 20 ppb (not shown). This suggests from O_3 formation is VOC during this episode in most of the MCMA urban area, consistent with the conclusion from $P(O_x)$ analyses in Sect. 3.2.2.

It can be noticed from Fig. 12 that the area where the ozone formation enhances most due to the 50% reduction in NOx emissions is not located in the high O_3 center (c.f. Fig. 2 lower left panel), but is shifted to the north of the O_3 center (i.e. closer to the source region than O_3 does). This suggests that the ozone formation has been depressed by the high NO_x concentration in the reference case on 15 April (on 14 April as well, see Fig. 11) in this area, which is consistent with the accelerated and enhanced O_3 formation shown in Fig. 11. Figure 13 shows the predicted distribution of NO_z/NO_y ratio in the base case averaged from 12:00 to 17:00 CDT on 15 April for the model bottom layer. The ratio of NO_z/NO_y reflects the chemical aging of an air plume: a chemically aged plume possesses higher NO_z/NO_y ratios and vice-versa. Values of NO_z/NO_y are also affected by advection and dispersion, deposition, and the reactive inhomogeneity of different VOCs. Figures 12 and 13 indicate that the VOC-sensitive area in the city generally coincides with the area of lower NO_z/NO_y ratios; the VOC-sensitive area matches well with areas with NO_z/NO_y ratios lower than 0.3. This characteristics also holds for areas of increasing $P(O_x)$ with decreasing NO_x emissions on 13–14 April. It is noticed that the area where O_3 poses the largest increase due to the NO_x-only emissions reduction (not shown, but similar to Fig. 13) is also shifted to the north. This phenomenon may also suggest that photochemical aging plays an important role in af-

fecting the NO_x-VOC sensitivity of ozone formation. In a NO_x-rich environment, ozone formation is depressed in the immediate pollution source area (due to the NO titration and the "poisonous" OH+NO_2 reaction) until the plume travels a substantial distance to the downwind area. A reduction in NO_x emissions alleviates or even eases the depression in the immediate downwind area in the NO_x-saturated environment. These suggest that plume evolution history plays an important role in affecting the NO_x-VOC sensitivity of O_3 formation. The stagnant conditions during this period contribute to the VOC-sensitive chemistry.

Figure 14 shows the peak O_3 change for a 50% reduction in emissions of VOCs and of both NO_x and VOCs, respectively. In both scenarios peak O_3 concentrations decrease throughout the MCMA, with the former resulting in a larger degree of decrease of peak O_3. This result also suggests that O_3 formation is VOC-sensitive in the MCMA during this episode. The largest decrease in O_3 induced by the VOC emission reduction (see Fig. 14a) corresponds to the high O_3 area of the reference case. This should be contrasted with the NO_x-only reduction case.

Responses of near-surface $P(O_x)$ to emissions reductions in NO_x and VOC emissions, respectively, as a function of reference NO_x are summarized in Fig. 15. In Fig. 15 model data from 12:00–17:00 CDT 13–15 April in the REP-8 stations are used. We present here the response of $P(O_x)$, instead of O_3 itself, because the former provides more insights on the chemistry of O_3 formation and its relationship with O_3 precursors. It shows that under "all" NO_x conditions sampled (all points with NO_x concentrations fall in the range shown in the figure), a reduction in VOC emissions always leads to a decrease in $P(O_x)$, which also changes with NO_x. The dependence of the $P(O_x)$ change on NO_x due to the reduction of NO_x emissions is complicated. At NO_x less than ~12 ppb, $P(O_x)$ decreases when NO_x emissions are reduced; at NO_x levels of 15–25 ppb, the reduction of NO_x emissions can lead to either a decrease or increase of $P(O_3)$, due to the diverse $P(O_x)$-NOx relationship discussed previously; but at higher levels of NO_x (>30 ppb), the reduction of NO_x emissions results in an increase of $P(O_x)$. Despite the scatter of the $P(O_x)$ responses to reductions in NO_x and VOCs, it appears

that VOC emission control is more effective than the NO_x emission control at most NO_x levels. This statement is drawn from Fig. 15, i.e., from the simulated results in the REP-8 stations and in terms of the ozone production rate. The conclusion may be different when different regions are targeted. Replacing $P(O_x)$ with O_3, a graph similar to Fig. 15, with a different variability, is obtained. The difference is that $P(O_x)$ may be considered a present state quantity, while O_3 not only explicitly includes the influences of physical processes (e.g., transport and deposition), but also carries the history of the air mass (Kleinman, 2000).

These sensitivity calculations are necessarily based on the reference emissions. O_3 response to emissions reductions may vary with different base emissions because the O_3 sensitivity chemistry can shift from one regime to another regime. Certainly an accurate EI is a must and prerequisite in order to develop an O_3 control strategy based on sensitivity studies. In addition, the O_3 sensitivity chemistry may vary if the magnitude of emissions reduction changes (e.g., 30% or 70% reduction instead of 50% reduction). Finally, the O_3 sensitivity chemistry can behave differently under different meteorological situations, and thus in different regions. Future work will extend the sensitivity analyses to other two meteorological categories that also occur frequently in MCMA, "O_3 -North" and "Cold Surge", and to improved base EIs with different perturbations.

4 Conclusions and remarks

A 3-D chemical transport model (CAMx 4.03) was used to characterize ozone formation and its response to precursor changes in the MCMA during a 3-day episode of 13–15 April 2003. Model performance was assessed by comparing simulated near-surface O_3, NO_x, CO, and VOC concentrations with a comprehensive array of available measurements at the RAMA monitoring stations and at the CENICA supersite obtained during the MCMA-2003 field campaign. The model successfully reproduces the concentrations of CO, NO_x, O_3 and VOCs in the MCMA during this episode.

The relationship between O_3 production and ambient NO_x and VOC concentrations

was shown to be complex. This complexity is mainly attributable to the heterogeneous primary radical sources under different NO_x levels. The behavior of $P(O_x)$ suggests that O_3 formation is VOC limited during 12:00–17:00 CDT in the urban region. The model predicts O_3 photochemical formation rates of 10–80 ppb/h at the most frequently measured NO_x concentrations. These NO_x concentrations are much higher than in most U.S. urban regions. The high O_3 production is due to the high VOC reactivity, in which alkanes, alkenes, and aromatics make comparable contributions. The predicted ozone production efficiency is between 4–10 O_3 molecules per NO_x molecule oxidized, increasing with higher VOC-to-NO_2 reactivity.

Contributions of chemistry, transport, and deposition to O_3 production in the boundary layer are apportioned in this study. O_3 is produced photochemically during the day, and is transported to the free troposphere (via vertical advection) in the later afternoon and evening. Deposition has negligible effects on the column ozone within the boundary layer. Significant outflows of pollutants such as O_3 and PAN from the urban areas to the surrounding environment are predicted. This outflow can have important influences on the air quality on the regional scale. PAN is not in equilibrium during the photochemically active periods.

The response of O_3 production to reductions in precursor emissions was investigated using three emissions control scenarios: a 50% reduction in NO_x only, a 50% reduction in VOCs only, and 50% reductions in both NO_x and VOCs. 50% reductions in emissions of VOC-only and in both NO_x and VOCs lead to decreases of peak O_3, with the former reducing O_3 most. A 50% reduction in NO_x emissions leads to small decreases, or even increases in peak O_3 for less aged ($NO_z/NO_y<0.3$) urban plumes. These results suggest that O_3 formation in the midday during this episode is VOC sensitive in most of the city. The sensitivity evolves with time of the day.

The results obtained from model simulations are based on one meteorological event and one adjusted base emission scenario. Because of the possible uncertainties in the emissions inventory and the diverse response of O_3 to ambient precursor levels, and the sensitivity of the concentration of spatial distribution to meteorology; one

episodic simulation may not be sufficient to capture the general features of O_3-NO_x-VOC chemistry under a specific meteorological condition. More episodic studies are needed to construct a comprehensive and representative picture of the O_3 production characteristics and its response to emission controls. Future studies will be performed using upgraded initial base EIs (including improved adjustments, refined and improved spatial and temporal distributions) and different degree of emission controls under different meteorological conditions (including same meteorological categories but different episodes), such as those identified during the MCMA-2003 campaign, the "O_3-North"and "Cold Surge".

Acknowledgements. This research was supported by the Mexican Metropolitan Environmental Commission, the U.S. National Science Foundation (and ATM-308748 and 0528227), and the Department of Energy (Award DE-FG02-05ER3980). The authors thank operators and analyst personnel of the RAMA monitoring network for their contribution in gathering the data used in this manuscript. We are grateful to B. Lamb and E. Velasco for providing VOC canister sampling data and P. Sheehy for assistance in DOAS data processing. We also thank F. San Martini, E. Velasco, B. Lamb, G. Sosa and A. Garcia for their valuable discussions and comments. CAMx is made publicly available by ENVIRON, and the authors would like to thank G. Yarwood for his support.

References

Arriaga-Colina, J. L., West, J. J., Sosa, G., Escalona, S. S., Ordúñez, R. M., and Cervantes, A. D. M.: Measurements of VOCs in Mexico City (1992–2001) and evaluation of VOCs and CO in the emissions inventory, Atmos. Environ., 38, 2523–2533, 2004.

Acker, K., Moller, D., Wieprecht, W., Meixner, F. X., Bohn, B., Gilge, S., Plass-Dulmer, C., and Berresheim, H.: Strong daytime production of OH from HNO2 at a rural mountain site, Geophys. Res. Lett., 33, L02809, doi:10.1029/2005GL024643, 2006.

Baumgardner, D., Raga, G. B., Kok, G., Ogren, J., Rosas, I., Báez, A., and Novakov, T.: On the evolution of aerosol properties at a mountain site above Mexico City, J. Geophys. Res., 105, 22 243–22 254, 2000.

CAM (Comisión Ambiental Metropolitana): Inventario de Emisiones 2002 de la Zona Metropolitana del Valle de México. México, 2004.

Carter, W. P. L.: Documentation of the SAPRC-99 chemical mechanism for VOC reactivity, final report to California Air Resources Board, Contract 92-329 and 95-308, Calif. Air Res. Board, Sacramento, Calif., 2000.

Carter, W. P. L.: Environmental chamber studies of ozone formation potentials of volatile organic compounds, in: Proceedings of the NATO Advanced Research Workshop "Environmental Simulation Chambers: Application to Atmospheric Chemical Processes", edited by: Rudzinski, K. and Barnes, I., NATO Sciences Series, IV. Earth and Environmental Sciences, Zakopane, Poland, Kluwer Academic Publishers, 1–4 October 2004.

Castro, T., Madronich, S., Rivale, S., Muhlia, A., and Mar, B.: The influence of aerosols on photochemical smog in Mexico City, Atmos. Environ., 35, 1765–1772, 2001.

Chameides, W. L., Lindsay, R. W., Richardson, J., and Kiang, C. S.: The role of biogenic hydrocarbons in urban photochemical smog – Atlanta as a case-study, Science, 241, 1473–1475, 1988.

Chang, J. S., Brost, R. A., Isaksen, I. S. A., Madronich, S., Middleton, P., Stockwell, W. R., and Walcek, C. J.: A three-dimensional Eulerian acid deposition model: Physical concepts and formulation, J. Geophys. Res., 81, 421–423, 1987.

Daum, P. H., Kleinman, L. I., Imre, D. G., Nunnermacker, L. J., and Lee, Y.-N.: Springston, S. R., Newman, L., and Weinstein-Lloyd, J.: Analysis of the processing of Nashville urban emissions on July 3 and July 18, 1995, J. Geophys. Res., 105, 9155–9164, 2000.

Daum P. H., Kleinman, L. I., Springston, S. R., Nunnermacker, L. J., Lee, Y.- N., Weinstein-Lloyd, J., Zheng, J., and Berkowitz, C. M.: A comparative study of O_3 formation in the Houston urban and industrial plumes during the 2000 Texas Air Quality Study, J. Geophys. Res., 108, 4715, doi:10.1029/2003JD003552, 2003.

de Foy, B., Caetano, E., Magana, V., Zitacuaro, A., Cardenas, B., Retama, A., Ramos, R., Molina, L. T., and Molina, M. J.: Mexico City basin wind circulation during the MCMA-2003 field campaign, Atmos. Chem. Phys., 5, 2267–2288, 2005.

de Foy, B., Clappier, A., Molina, L. T., and Molina, M. J.: Distinct wind convergence patterns due to thermal and momentum forcing of the low level jet into the Mexico City basin, Atmos. Chem. Phys., 6, 1249–1265, 2006a.

de Foy, B., Molina, L. T., and Molina, M. J.: Satellite-derived land surface parameters for mesoscale modeling of the Mexico City basin, Atmos. Chem. Phys., 6, 1315–1330, 2006b.

Doran, J. C. and Zhong, S.: Thermally driven gap winds into the Mexico City basin, J. Appl. Meteorol., 39, 1330–1340, 2000.

Doran, J. C., Abbott, S., Archuleta, J., Bian, X., Chow, J., Coulter, R. L., de Wekker, S. F. J., Edgerton, S., Elliott, S., Fernandez, A., Fast, J. D., Hubbe, J. M., King, C., Langley, D., Leach, J., Lee, J. T., Martin, T. J., Martinez, D., Martinez, J. L., Mercado, G., Mora, V., Mulhearn, M., Pena, J. L., Petty, R., Porch, W., Russell, C., Salas, R., Shannon, J. D., Shaw, W. J., Sosa, G., Tellier, L., Templeman, B., Watson, J. G., White, R., Whiteman, C. D., and Wolfe, D.: The15 IMADA-AVER boundary layer experiment in the Mexico City area, Bull. Am. Meteorol. Soc., 79, 2497–2508, 1998.

Edgerton, S. A., Bian, X., Doran, J. C., et al.: Particulate Air Pollution in Mexico City: A Collaborative Research Project, J. Air Waste Manage. Assoc., 49, 1221–1229, 1999.

ENVIRON: User's Guide Comprehensive Air Quality Model with Extension (CAMx) Version 4.03. ENVIRON International Coporation, Novato, available at http://www.camx.com, California, 2003.

Fast, J. D. and Zhong, S.: Meteorological factors associated with inhomogeneous ozone concentrations within the Mexico City basin, J. Geophys. Res., 103, 18 927–18 946, 1998.

Finlayson-Pitts, B. J., Wingen, L. M., Summer, A. L., Syomin, D., and Ramazan, K. A.: The heterogeneous hydrolysis of NO_2 in laboratory systems and in outdoor and indoor atmospheres: An integrated mechanism, Phys. Chem. Chem. Phys., 5, 223–242, 2003.

Fine, J., Vuilleumier, L., Reynolds, S., Roth, P., and Brown, N.: Evaluating uncertainties in regional photochemical air quality modeling, Ann. Rev. Environ. Resour., 28, 59–106, 2003.

Gaffney, J. S., Marley. N. A., Cunningham, M. M., and Doskey, P. V.: Measurements of peroxyacyl nitrates (PANS) in Mexico City: implications for megacity air quality impacts on regional scales, Atmos. Environ., 33, 5003–5012, 1999.

Garcia, A. R., Volkamer, R., Molina, L. T., Molina, M. J., Samuelson, J., Mellqvist, J., Galle, B., Herndon, S. C., and Kolb, C. E.: Separation of emitted and photochemical formaldehyde in Mexico City using a statistical analysis and a new pair of gas-phase tracers, Atmos. Chem. Phys. Discuss., 5, 11 055–11 090, 2005.

Gobierno del Distrito Federal (GDF): Informe del Estado de la Calidad del Aire y Tendencias 2003 para la Zona Metropolitana del Valle de México, (Dirección Generalde Gestión Ambiental del Aire, México, D. F., 2004).

Grell, G. A., Dudhia, J., and Stauffer, D. R.: A Description of the Fifth-Generation Penn State/NCAR Mesoscale Model (MM5), Tech. Rep. NCAR/TN-398+STR, NCAR, 1995.

IMP (Instituto Mexicano el Petróleo): Investigación sobre materia particulada y deterioro atmosférico, Subdirección de Protección Ambiental, 1994–1998, 1998.
Jazcilevich, A. D., Garcia, A. R., and Caetano, E.: Locally induced surface air confluence by complex terrain and its effects on air pollution in the valley of Mexico, Atmos. Environ., 39, 5481–5489, 2005.
Kleffmann, J., Becker, K. H., and Wiesen, P.: Heterogeneous NO_2 conversion processes on acid surfaces: Possible atmospheric implications, Atmos. Environ., 32, 2721–2729, 1998.
Kleinman, L. I.: Ozone process insights from field experiments – part II: Observation-based analysis for ozone production, Atmos. Environ., 34, 2023–2033, 2000.
Kleinman, L. I., Daum, P. H., Lee, J. H., Lee, Y.-N., Nunnermacker, L. J., Springston, S. R., Newman, L., Weinstein-Lloyd, J., and Sillman, S.: Dependence of ozone production on NO and hydrocarbons in the troposphere, Geophys. Res. Lett., 24, 2299–2302, 1997.
Kleinman, L. I., Daum, P. H., Imre, D., Lee, Y.-N., Nunnermacker, L. J., Springston, S. R., Weinstein-Lloyd, J., and Rudolph, J.: Ozone production rate and hydrocarbon reactivity in 5 urban areas: A cause of high ozone concentration in Houston, Geophys. Res. Lett., 29(10), 1467, doi:10.1029/2001GL014569, 2002.
Kleinman L. I., Daum, P. H., Lee, Y.-N., Nunnermacker, L. J., Springston, S. R., Weinstein-Lloyd, J., and Rudolph, J.: A comparative study of ozone production in five U.S. metropolitan areas, J. Geophys. Res., 110, D02301, doi:10.1029/2004JD005096, 2005.
Kolb, C. E., Herndon, S. C., McManus, J. B., Shorter, J. H., Zahniser, M. S., Nelson, D. D., Jayne, J. T., Canagaratna, M. R., and Worsnop, D. R.: Mobile laboratory with rapid response instruments for real-time measurements of urban and regional trace gas and particulate distributions and emission source characteristics, Environ. Sci., Technol., 38, 5694–5703, 2004.
LANL/IMP (Los Alamos National Laboratory and Instituto Mexicano del Petróleo): Mexico City Air quality Research Initiative, Los Alamos, NM, 1994.
Lei, W., Zhang, R., Tie, X., and Hess, P.: Chemical characterization of ozone formation in the Houston-Galveston area: A chemical transport model study, J. Geophys. Res., 109, D12301, doi:10.1029/2003JD004219, 2004.
Liu, S. C., Trainer, M., Fehsenfeld, F. C., Parrish, D. D., Williams, E. J., Fahey, D. W., Hubler, G., and Murphy, P. C.: Ozone production in the rural troposphere and the implications for regional and global ozone distributions, J. Geophys. Res., 92, 4191–4207, 1987.
Madronich, S. and Flocke, S.: The role of solar radiation in atmospheric chemistry, in: Handbook of Environmental Chemistry, edited by: Boule, P., p. 1–26, Springer-Verlag, Heidelberg, Germany, 1998.
Marley, N. A., Gaffney, J. S., White, R. V., Rodriguez-Cuadra, L., Herndon, S. E., Dunlea, E., Volkamer, R. M., Molina, L. T., and Molina, M. J.: Fast gas chromatography with luminol chemiluminescence detection for the simultaneous determination of nitrogen dioxide and peroxyacetyl nitrate in the atmosphere, Rev. Sci. Instrum. 75, 4595–4605, 2004.
Molina, L. T. and Molina, M. J. (Eds.): Air Quality in the Mexico Megacity: An integrated Assessment, Kluwer Academic Publishers, 2002.
Molina, M. J. and Molina, L. T.: Megacities and Atmospheric Pollution, J. Air Manage. Assoc., 54, 644–680, 2004.
Molina, L. T., Molina, M. J., Slott, R. S., Kolb, C. E., Gbor, P. K., Meng, F., Singh, R. B., Galvez, O., Sloan, J. J., Anderson, W. P., Tang, X. Y., Hu, M., Xie, S., Shao, M., Zhu, T., Zhang, Y. H., Gurjar, B. R., Artaxo, P. E., Oyola, P., Gramsch, E., Hidalgo, D., and Gertler, A. W.: 2004 Critical Review online version: Air Quality in Selected Megacities, http://www.awma.org, 2004.
Nunnermacker, L. J., Imre, D., Daum, P. H., Kleinman, L., Lee, Y.-N., Lee, J. H., Springston, S. R., Newman, L., Weinstein-Lloyd, J., Luke, W. T., Banta, R., Alvarez, R., Senff, C., Sillman, S., Holdren, M., Keigley, G. W., and Zhou, X.: Characterization of the Nashville urban plume on July 3 and July 18, 1995, J. Geophys. Res., 103, 28 129–28 148, 1998.
Odum, J. R., Hoffmann, T., Bowman, F., Collins, D., Flagan, R. C., and Seinfeld, J. H.: Gas/Particle Partitioning and Secondary Organic Aerosol Yields, Environ. Sci. Technol., 30, 2580–2585, 1996.
Raga,G. B., Baumgardnera, D., Castroa, T., Martínez-Arroyoa, A., and Navarro-González, R.: Mexico City air quality: a qualitative review of gas and aerosol measurements (1960–2000), Atmos. Environ., 35, 4041–4058, 2001.
Rogers, T. M., Grimsruda, E. P., Herndon, S. C., et al.: On-road measurements of volatile organic compounds in the Mexico City Metropolitan Area using proton transfer reaction mass spectrometry, International J. Mass Spectrom., 252(1), 26–37, 2006.
Russell, A. and Dennis, R.: NARSTO critical review of photochemical models and modeling, Atmos. Environ., 34, 2283–2324, 2000.
Salcedo, D., Dzepina, K., Onasch, T. B., et al.: Characterization of Ambient Aerosols in Mexico City during the MCMA-2003 Campaign with Aerosol Mass Spectrometry – Part I: Quantification, Shape-Related Collection Efficiency, and Comparison with Collocated Instruments,

Atmos. Chem. Phys. Discuss., 5, 4143–4182, 2005a.
Salcedo, D., Dzepina, K., Onasch, T. B., et al.: Characterization of ambient aerosols in Mexico City during the MCMA-2003 campaign with Aerosol Mass Spectrometry – Part II: overview of the results at the CENICA supersite and comparison to previous studies, Atmos. Chem. Phys. Discuss., 5, 4183–4221, 1995.
Seinfeld, J. H. and Pandis, S. N.: Atmospheric Chemistry and Physics: From Air Pollution to Climate Change, John Wiley & Sons, New York, 1998.
Shirley, T. R., Brune, W. H., Ren, X., Mao, J., Lesher, R., Cardenas, B., Volkamer, R., Molina, L. T., Molina, M. J., Lamb, B., Velasco, E., Jobson, T., and Alexander, M.: Atmospheric oxidation in the Mexico City Metropolitan Area (MCMA) during April 2003, Atmos. Chem. Phys., 6, 2753–2765, 2006.
Sillman, S., Logan, J. A., and Wofsy, S. C.: The sensitivity of ozone to nitrogen oxides and hydrocarbons in regional ozone episodes, J. Geophys. Res., 95, 1837–1851, 1990.
Sillman, S.: The use of NOy, H_2O_2, and HNO_3 as indicators for ozone-NOx-hydrocarbon sensitivity in urban locations, J. Geophys. Res., 100, 14 175–14 188, 1995.
Sillman, S.: The relation between ozone, NO_x and hydrocarbons in urban and polluted rural environments, Atmos. Environ., 33, 1821–1845, 1999.
St. John, J. C., Chameides, W. L., and Saylor, R.: Role of anthropogenic NO_x and VOC as ozone precursors: A case study from the SOS Nashville/Middle Tennessee Ozone Study, J. Geophys. Res., 103, 22 415–22 424, 1998.
Streit, G. E. and Guzmán, F.: Mexico City Air quality: Progress of an international collaborative project to define air quality management options, Atmos. Environ., 30, 723–733, 1996.
Stutz, J., Alicke, B., Ackermann, R., Geyer, A., Wang, S., White, A. B., Williams, E. J., Spicer, C. W., and Fast, J. D.: Relative humidity dependence of HONO chemistry in urban areas, J. Geophys. Res., 109, D03307, doi:10.1029/2003JD004135, 2004.
Tonnesen, G. S. and Dennis, R. L.: Analysis of radical propagation efficiency to assess ozone sensitivity to hydrocarbons and NO_x. 1. Local indicators of instantaneous odd oxygen production sensitivity, J. Geophys. Res., 105, 9213–9226, 2000.
Velasco, E., Lamb, B., Pressley, S., Allwine, E., Westberg, H., Jobson, T., Alexander, M., Prazeller, P., Molina, L., and Molina, M.: Flux measurements of volatile organic compounds from an urban landscape, Geophys. Res. Lett., 32, L20802, doi:10.1029/2005GL023356, 2005.
Velasco, E., Lamb, B., Westberg, H., Allwine, E., Sosa, G., Arriaga, J. L., Jonson, T., Alexander,

M., Prazeller, P., Knighton, B., Rogers, T. M., Grutter, M., Herndon, S. C., Kolb, C. E., Zavala, M., de Foy, B., Molina, L. T., and Molina, M. J.: Distribution, magnitudes, reactivities, ratios and diurnal patterns of volatile organic compounds in the Valley of Mexico during the MCMA 2002 & 2003 field campaigns, Atmos. Chem. Phys. Discuss., 6, 7563–7621, 2006.
Volkamer, R., Molina, L. T., Molina, M. J., Shirley, T., and Brune, W. H.: DOAS measurement of glyoxal as an indicator for fast VOC chemistry in urban air, Geophys. Res. Lett., 32, L08806, doi:10.1029/2005GL022616, 2005.
West, J. J., Zavala, M. A., Molina, L. T., Molina, M. J., San Martini, F., McRae, G. J., Sosa-Iglesias, G., and Arriaga-Colina: J. L.: Modeling ozone photochemistry and evaluation of hydrocarbon emissions in the Mexico City metropolitan area, J. Geophys. Res., 109, D19312, doi:10.1029/2004JD004614, 2004.
Whiteman, C. D., Zhong, S., Bian, X., Fast, J. D., and Doran, J. C.: Boundary layer evolution andregional-scale diurnal circulations over the Mexico Basin and Mexican Plateau, J. Geophys. Res., 105, 10 081–10 102, 2000.
Williams, M. D., Brown, M. J., Cruz, X., Sosa, G., and Streit, G.: Development and testing of meteorology and air dispersion models for Mexico City, Atmos. Environ., 29, 2929–2960, 1995.
Zavala, M., Slott, R., S, Dunlea, E. J., Marr, L., Molina, L. T., Molina, M. J., Herndon, S. C., Shorter, J. H., Zahniser, M., Kolb, C. E., Knighton, B., and Rogers, T: Characterization of on-road vehicle emissions in the Mexico City Metropolitan Area using a mobile laboratory in chase and fleet average measurement modes during the MCMA-2003 field campaign, Atmos. Chem. Phys. Discuss., 6, 4689–4725 2006.

Table 1. Total annual emissions (in ktons/year) by source category in the MCMA from the 2002 official emission inventory.

	CO	NO_x	VOCs[a]	VOC[b]
Mobile	1927.1	156.3	193.8	332.3
Area	4.4	6.5	258.9	439.7
Point	6.9	19.5	75.2	112.8
Vegetation and soil	N/A	0.6	16.6	15.2
Total	1938.4	183.0	544.5	900.0

[a] Initial estimates from MCMA 2002EI.
[b] Adjusted estimates.

Table 2. Adjustment factors for correction of the 2002 MCMA emissions inventory.

Model species	Adjustment factor $^{+}$ (this work)	Adjustment factor $^{\#}$ from Velasco et al. (2006)
Ethane		2.3 (see note)
ALK1	2.0	3.1 (see note)
ALK2	3.0	0.3 (see note)
ALK3	4.0	
ALK4	1.5	
ALK5	0.4	
ETHE	1.0	
OLE1	1.0	0.4
OLE2	1.0	0.2
ARO1	1.5	0.6
ARO2	1.5	0.7
HCHO	9.0	
CCHO and RCHO	4.0	

Note: different speciation of alkanes in CAMx and the work of Velasco et al were used. $ALK1^{+}$ contains ethane; $ALK2^{+}$ includes propane and acetylene; $ALK3^{+}$ includes n-butane, i-butane and 2,2-dimethyl butane; $ALK4^{+}$ includes i-pentane, n-pentane, cyclopentane, methylcyclopentane,2-methyl pentane, 3-methyl pentane, 2,3-dimethyl butane and hexane; $ALK5^{+}$ includes cyclohexane, 2-methyl hexane, 3-methyl hexane, 2,3-dimethyl pentane, 2-methyl heptane, 4-methyl heptane, i octane, n-heptane, methylcyclohexane, 2,4-dimethyl hexane, 2,3,4-trimethyl heptane, n-octane, nonane and 1,2,4 trimethylcyclohexane. $ALK1^{\#}$ is the combination of $ALK2^{+}$, $ALK3^{+}$ and $ALK4^{+}$; $ALK2^{\#}$ corresponds to $ALK5^{+}$.

Table 3. Notation.

Symbol	Meaning
P_G	Gross chemical production rate
P	Net chemical production rate
L	Net chemical loss rate
Q	Radical primary sources
PFR	Peroxide formation rate
L_R	Radical loss rate due to radical-radical reactions of $OH+HO_2$ and $RO_2+R'O_2$
L_N	Formation rate of PANs, other organic nitrates, and particulate nitrates
K_{VOC}	VOC reactivity, defined as the product of the VOC concentration and the rate constant for the reaction of VOC+OH
K_{NO2}	NO2 reactivity, defined as the product of the NO2 concentration and the rate constant for the reaction of NO_2+OH
OPE	Ozone production efficiency, defined as $P(O_3)/P(NO_z)$

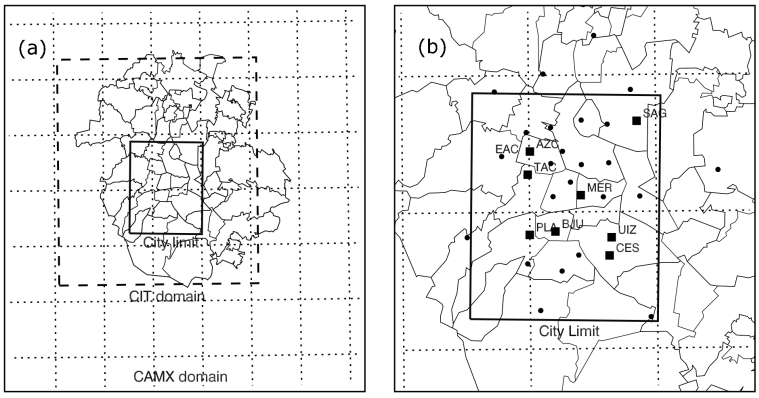

Fig. 1. (a) Model domain and **(b)** RAMA monitoring stations. Also shown in (a) are the CIT model domain (delimited by dashed-line) and the MCMA city limit or urban region (the inner bold square) where most RAMA monitoring stations are located. The RAMA monitoring stations are indicated as filled circles and filled squares. The 8 stations marked as filled squares with the station codes along side are denoted as REP-8 stations. The thin curves are the MCMA delegation borderlines.

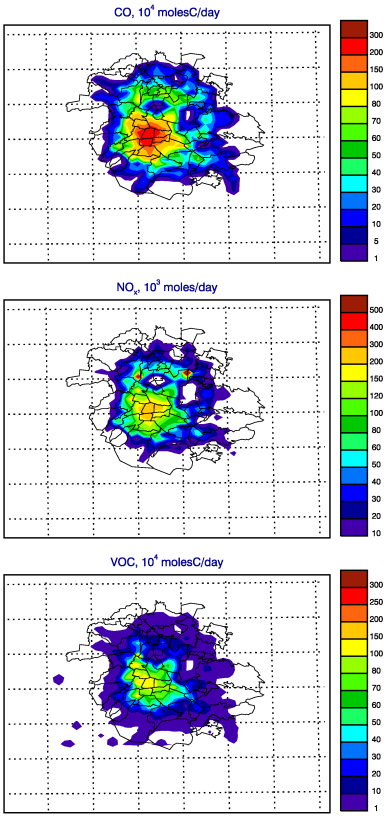

Fig. 2. Spatial distribution of CO, NO_x and VOC emissions for a normal weekday in the initial estimates from the 2002 official emission inventory.

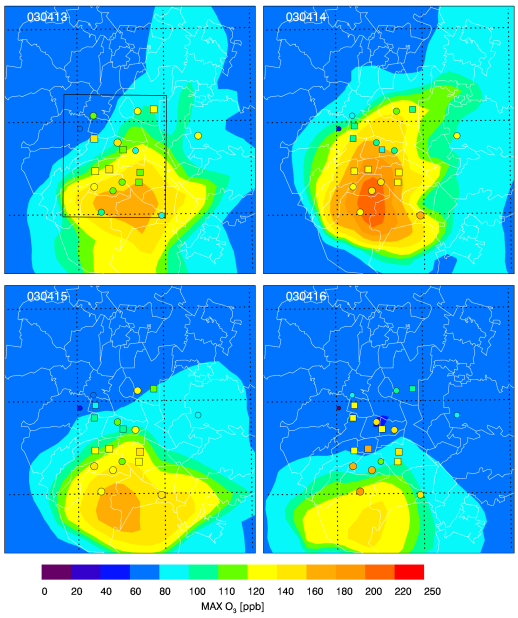

Fig. 3. Comparison of simulated (colored contour) versus observed (colored dots and squares) near-surface peak O_3 concentration during 13–16 April 2003. Dots and squares indicate the positions of RAMA monitoring stations which have O_3 observation data during this episode, whose size is proportional to the O_3 concentration.The REP-8 stations are marked as small suuares. Also shown in the upper left panel is the city limit (encompassed by a black rectangle) in which data are used for analyses.

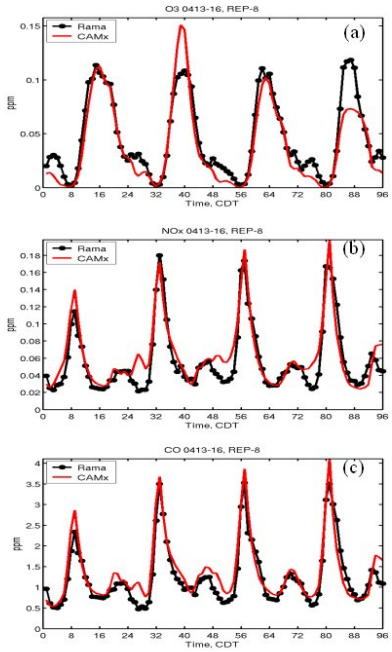

Fig. 4. Comparison of measured (black) and simulated (red) diurnal variation of near surface hourly concentrations of **(a)** O_3, **(b)** NO_x, and **(c)** CO averaged over 8 stations (marked as square in Fig. 1). Time in the x-axis is the end hour in CDT (central daylight time) starting at 01:00 CDT 13 April 2003.

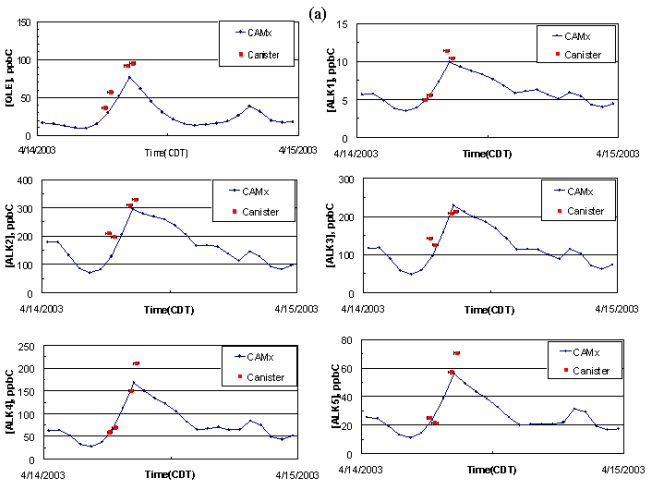

Fig. 5. Comparisons of modeled VOC concentrations **(a)** with canister data, and **(b)** DOAS measurements at CENICA. Canister data are 30-min averages. ARO1 in the DOAS measurements is assumed to be benzene and toluene exclusively. A scale factor obtained from the canister data is applied to the DOAS data to construct ARO2 concentration. The legend G1NW denotes one model grid northwest of CENICA (3 km north and west respectively).

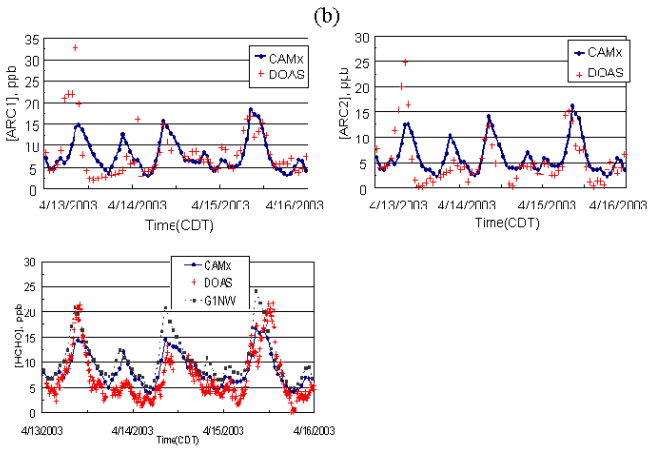

Fig. 5. Continued.

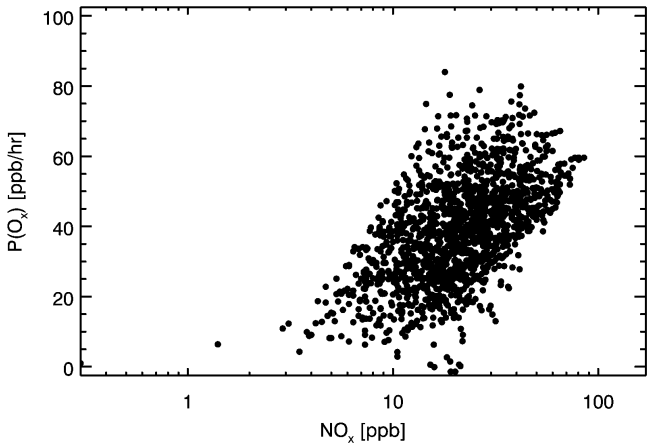

Fig. 6. Simulated dependence of photochemical production rates of O_x ($P(O_x)$) on NO_x in the model bottom layer over the urban region during 12:00–17:00 CDT, 13–15 April 2003.

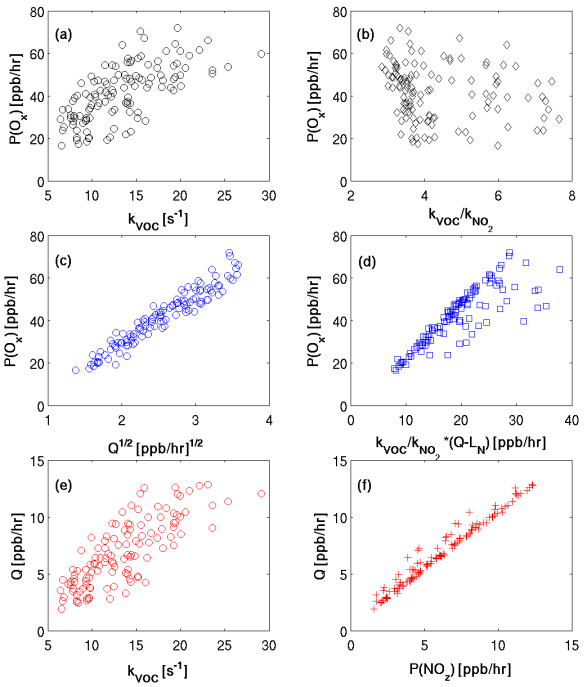

Fig. 7. Simulated relationships among O_x formation rate ($P(O_x)$), primary radical source (Q), and ratio of VOC-to-NO2 reactivity (k_{VOC}/k_{NO2}), and relationship between radical source as a function and VOC reactivity. Data are sampled at the REP-8 stations between 12:00–17:00 CDT 13–15 April 2003.

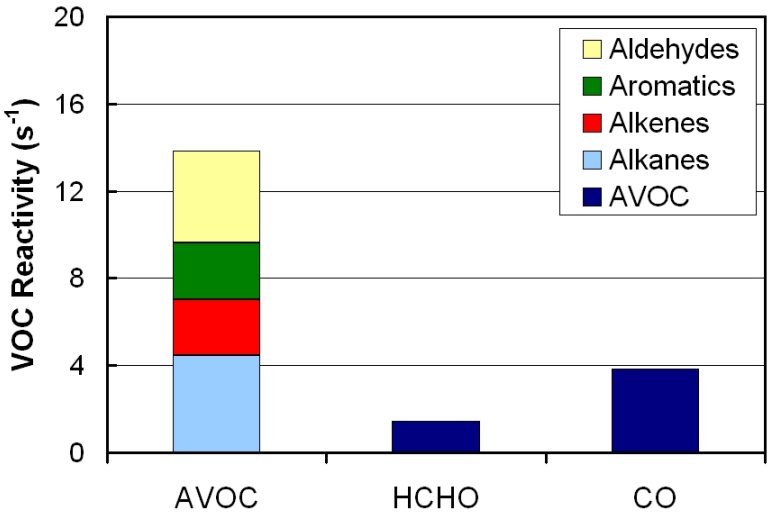

Fig. 8. Simulated VOC reactivity averaged over the REP-8 stations during 12:00–17:00 CDT 13–15 April 2003 at model bottom layer. AVOC = anthropogenic VOCs. Aldehydes include HCHO.

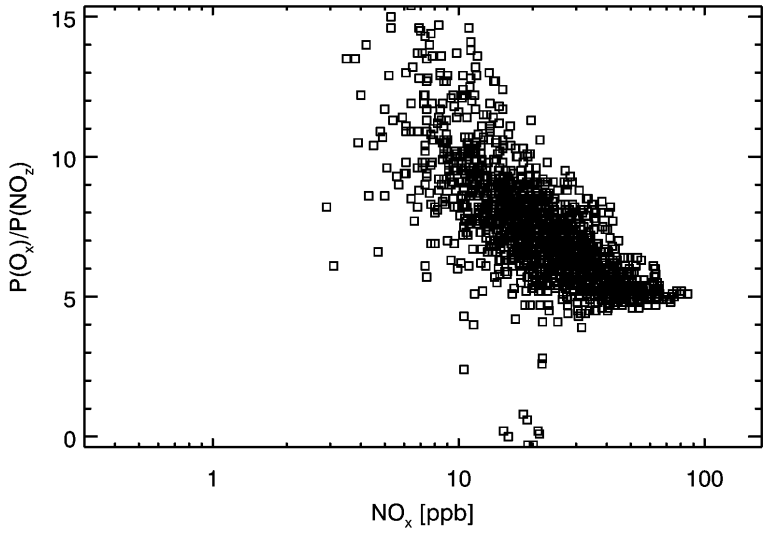

Fig. 9. Simulated relationship between ozone production efficiency ($P(O_x)$)/P((NO_z)) and NO_x at 12:00–17:00 CDT during 13–15 April 2003 in the model bottom layer over the urban region.

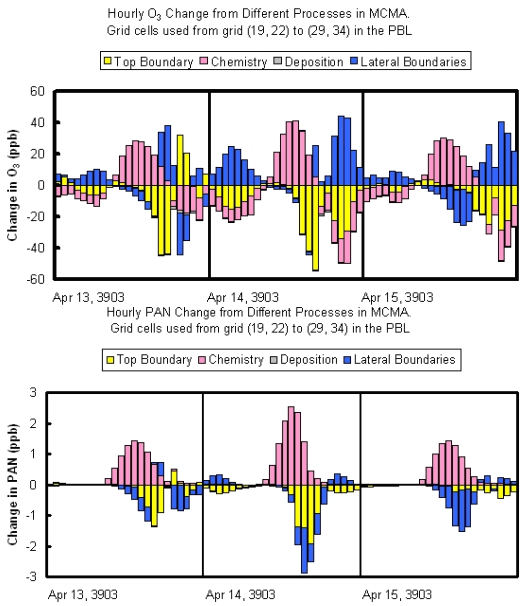

Fig. 10. Stacked time series of contribution of various processes to **(a)** O_3 production, and **(b)** PAN production in the simulated boundary layer. The analysis region is confined to the urban region, and bars are the hourly-integrated production rate change due to different processes within the PBL (each bar represents one hour).

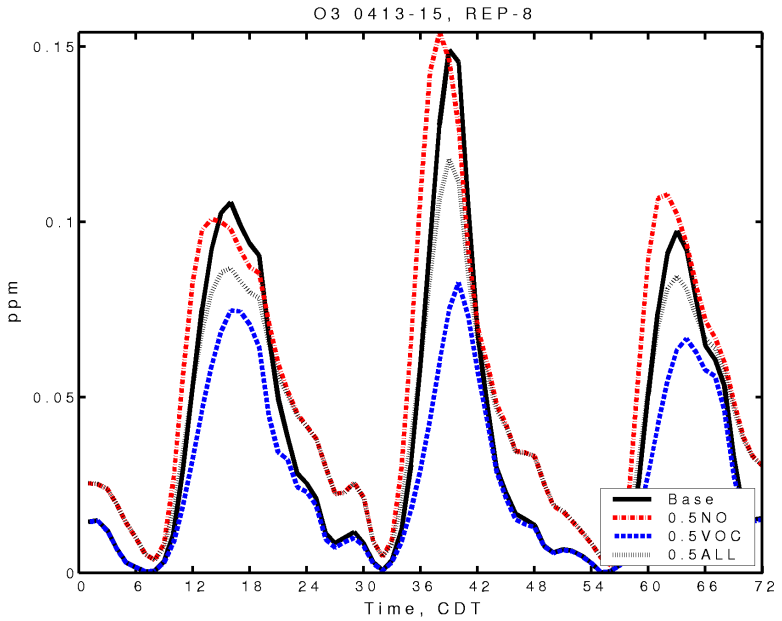

Fig. 11. Time series of O_3 concentrations for different emission control scenarios. Data are averaged over the REP-8 stations in the bottom model layer. Time starts at 00:00 CDT 13 April 2003. In the legend Base denotes the reference case, 0.5 NO denotes a 50% reduction in NO_x emissions, 0.5 VOC denotes a 50% reduction in VOC emissions, and ALL denotes a 50% reduction in emissions of both NO_x and VOCs.

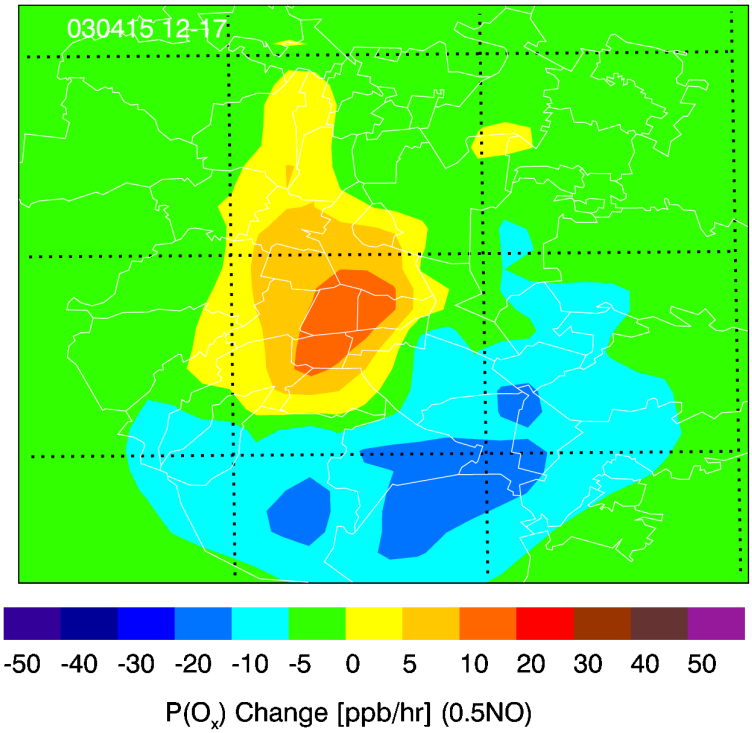

Fig. 12. Change of O_x photochemical production rate in the model bottom layer on 15 April 2003 due to a 50% reduction in NO_x emissions. Data are averaged over 12:00–17:00 CDT. The change is calculated as $P(O_x)$(emission control run) – $P(O_x)$(reference run).

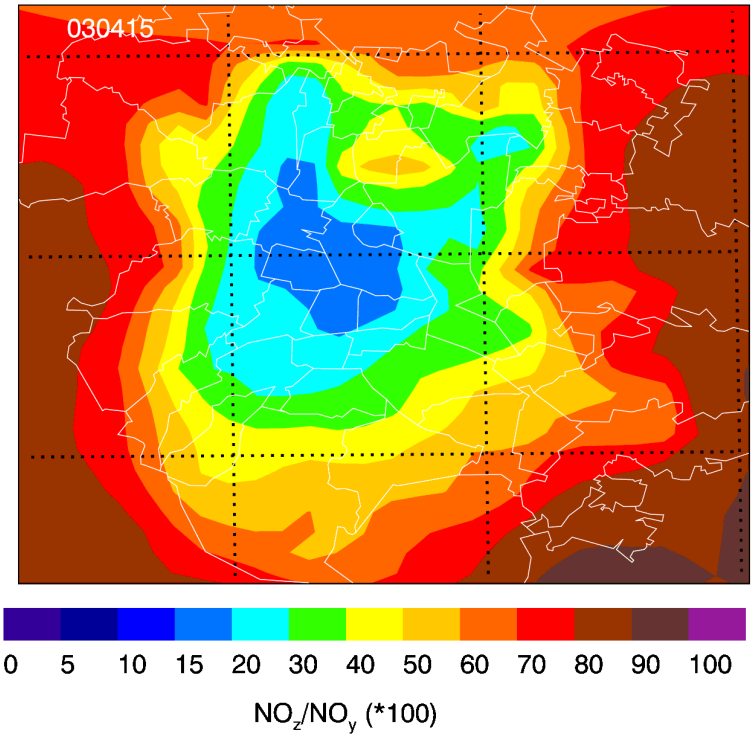

Fig. 13. Simulated geographic distribution of NO_z/NO_y ratio in the reference run averaged over 12:00–17:00 CDT on 15 April 2003 in the model bottom layer.

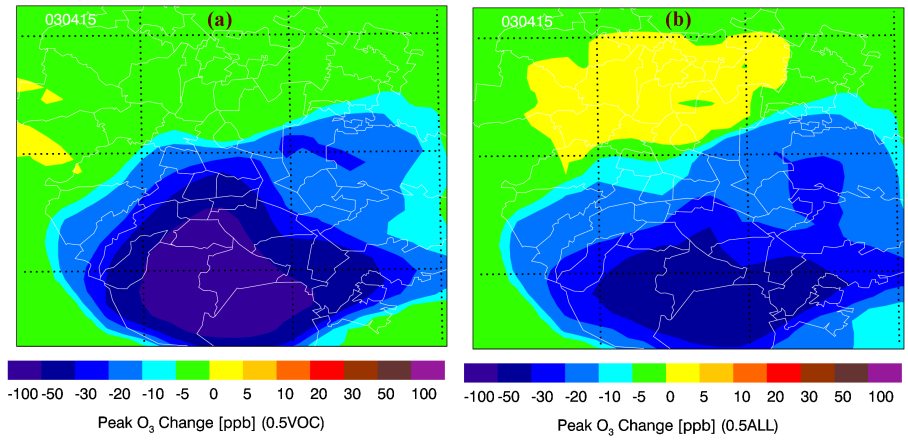

Fig. 14. Change of peak O_3 in the model bottom layer on 15 April 2003 due to a 50% reduction in the emissions of **(a)** VOCs only and **(b)** NO_x and VOCs both.

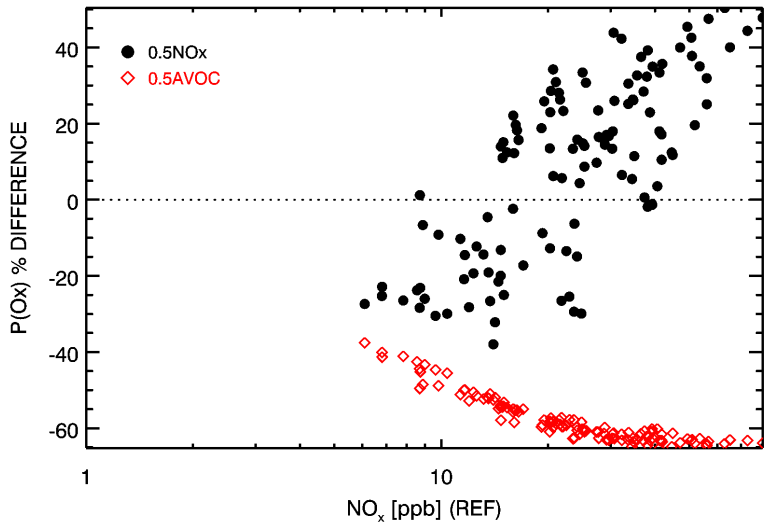

Fig. 15. The Percentage change of $P(O_x)$ as a function of reference NO_x from 13:00–17:00 CDT during 13–15 April 2003 in the bottom model layer over the REP-8 stations.